Journal of Structural Geology 30 (2008) 1218–1228

Contents lists available at ScienceDirect

Journal of Structural Geology

journal homepage: www.elsevier.com/locate/jsg

Crystallographic fabric development along a folded polycrystalline hematite

Luiz F.G. Morales*, Leonardo E. Lagoeiro, Issamu Endo

Departamento de Geologia, Universidade Federal de Ouro Preto, Campus Morro do Cruzeiro, s/n°. 35400-000 Ouro Preto, MG, Brazil

ARTICLE INFO

Article history:
Received 22 October 2007
Received in revised form 12 May 2008
Accepted 13 May 2008
Available online 21 May 2008

Keywords:
Hematite
Crystallographic preferred orientation
Electron backscattered diffraction
Grain size and shape analysis

ABSTRACT

Detailed analyses of microstructures and crystallographic preferred orientations (CPOs) of hematite rocks were conducted in samples of polycrystalline hematite around a tight fold in the Quadrilátero Ferrífero region, southeastern Brazil. Grain size is dominantly very fine in all samples (≈15–30 μm), with a slight increase toward the hinge. Grain aspect ratio increases substantially toward the hinge, from an average of 2 in the limb to 9 in the hinge. Distribution patterns of [0001] axes and poles of planes $\{10\bar{1}0\}$, $\{11\bar{2}0\}$ and $\{10\bar{1}4\}$ suggest that intracrystalline slip operate on the basal plane along the <a> direction. The distribution of the poles of prismatic planes parallel to the foliation of reference frame indicate that the all the symmetric <a>-slip directions of hematite crystals were equally efficient during activation of basal intracrystalline slip. Increasing aspect ratio is accompanied by CPO intensification toward the hinge, where intensification was aided during deformation by bulk rotation of the hematitic plates and possibly by some grain boundary sliding. Such CPO intensification with the increase of aspect ratio toward the hinge is used to infer that the fold developed by flexural flow.

1. Introduction

Development of crystallographic preferred orientation (CPO) in deformed rocks is generally attributed to intracrystalline deformation and dynamic recrystallization processes (e.g. Nicolas and Poirier, 1976; Schmid and Casey, 1986; Law et al., 1990; Lloyd et al., 1992; Ji et al., 1993). However, depending on the environmental conditions, other processes may accommodate strain, which, in some cases, can also result in a well-developed CPO fabric.

In the case of hematite-bearing rocks, the development of CPO seems to be related to two different processes. The first is dislocation-related process (e.g. Siemes et al., 2000), which for low metamorphic grade is dominated by basal <a> slip (Hennig-Michaeli, 1977; Siemes and Hennig-Michaeli, 1985; Siemes et al., 2000; Rosière et al., 2001). The resulting CPO can be intensified in shear zones or in folds by bulk rotation of hematite crystals (e.g. Cogné and Gapais, 1986). However, as preferred orientation data in hematite-bearing rocks was previously obtained through X-ray or neutron diffraction techniques (e.g. Siemes and Hennig-Michaeli, 1985; Siemes et al., 2000; Rosière et al., 2001), which do not permit a direct correlation between microstructures and lattice-preferred orientation. To fill this gap, we measured microstructures and crystallographic orientations using the electron backscattered diffraction in a scanning electron microscope (EBSD/SEM; Randle, 1992; Prior et al., 1999; Morales et al., 2007). The samples were collected from a folded iron formation in the northeastern part of Quadrilatero Ferrífero (QF) region, southeast Brazil. The studied rocks are polycrystalline hematite (also called "hematitites" here) sampled from the hinge and limbs of a decametric-scale fold. In this paper, we discuss microstructural and CPO observations in terms of the variations of CPO patterns and microstructures developed around the fold, and interpret these variations in terms of deformation and folding mechanisms.

2. Geological setting and description of the fold

The studied samples come from the Itabira Group, a sequence of metasedimentary rocks of Archean/Palaeoproterozoic ages (Babinski et al., 1995; Alkmim and Marshak, 1998), which host large iron ore bodies of hematitites and itabirites (Fig. 1). These rocks result from metamorphism of chemical-sedimentary rocks in which layers of varied thickness of quartz and magnetite/hematite aggregates alternate rhythmically, and are equivalent to the metamorphosed banded iron formations. The entire sequence was deformed and metamorphosed in three main deformation phases. Polyphase D_1 deformation was the most intense and is related to the recrystallization and formation of large iron-ore deposits in the Quadrilátero Ferrífero (QF) region. During this first episode of deformation, two sets of coaxial folds, affecting the original sedimentary layering developed during progressive deformation, concomitantly to the development of a pervasive axial-plane foliation (S_1) with intense shearing and local

* Corresponding author. Tel.: +55 31 3559 1600; fax: +55 31 3559 1606.
E-mail address: luiz_grafulha@yahoo.com.br (L.F.G. Morales).

0191-8141/$ – see front matter © 2008 Elsevier Ltd. All rights reserved.
doi:10.1016/j.jsg.2008.05.004

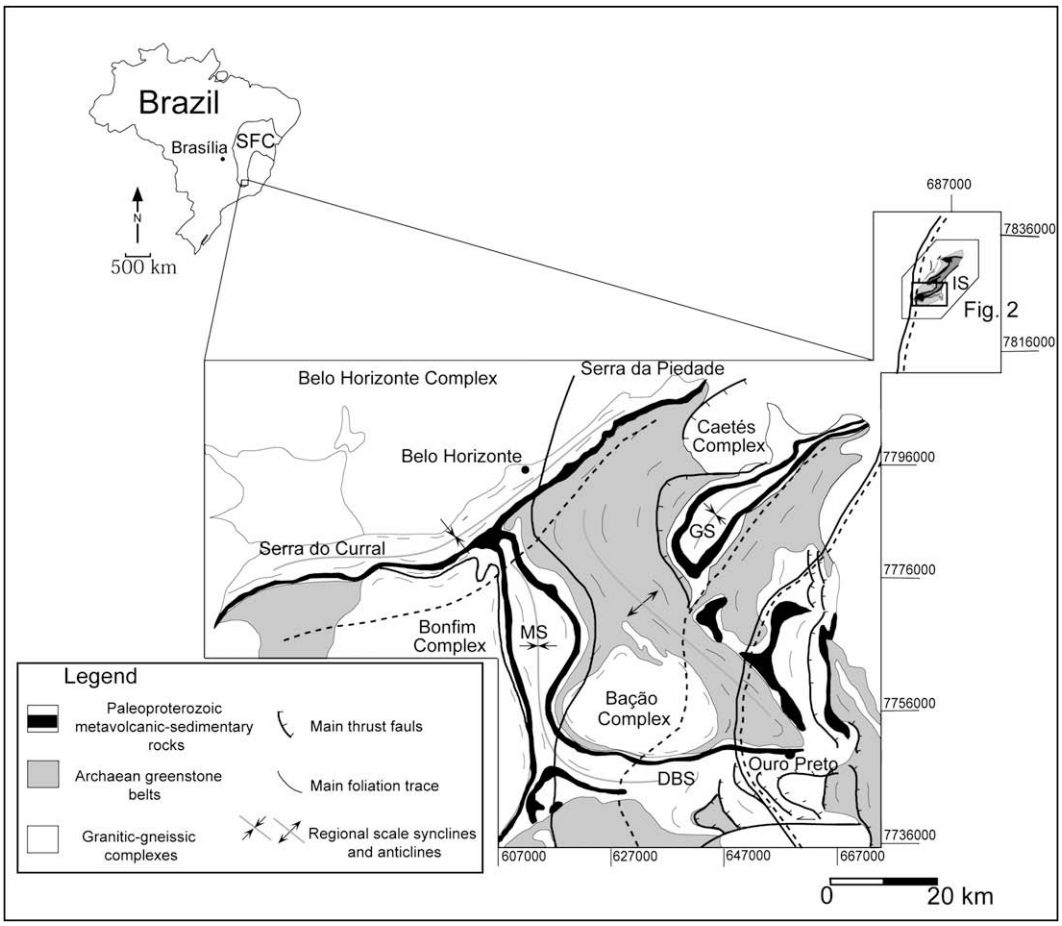

Fig. 1. Geological map of the Quadrilátero Ferrífero area, showing main geological units that are exposed in the region, and regional structures. The studied fold lies in the northeastern tip of the Quadrilátero Ferrífero region (marked by the black rectangle). SFC, São Francisco Craton; IS, Itabira Syncline; MS, Moeda Syncline; GS, Gandarela Syncline; DBS, Dom Bosco Syncline. Modified from Rosière et al. (2001).

transposition of the sedimentary layering (Lagoeiro et al., 2003; Almeida et al., 2005), The peak of metamorphism occurred during this deformation episode, and reached temperatures of the upper greenschist to lower amphibolite facies (Hoefs et al., 1982; Pires, 1995). Intense fluid percolation associated with deformation and metamorphism led to quartz leaching, breakdown of magnetite to hematite, and consequent enrichment of iron-oxide minerals in the iron formations (e.g. Lagoeiro, 1998; Rosière et al., 2001), producing relatively large deposits of hematitites. The eastern domain of the QF, where our samples were collected, is considered to have the greatest deformation due the superposition of Brasiliano (~650 Ma) structures over the Archaean/Paleoproterozoic ones (Rosière et al., 2001). In the high-strain domain, $L > S$ and $L = S$ tectonites are common either in hematitites or in the country rocks. Tight to isoclinal folds are also commonly observed in the eastern domain of the QF region and seem to have developed synchronously with the $L > S$ fabric in the aggregates, since they do not fold the fabric of the L-tectonites.

The second and third deformations (D_2 and D_3) were less intense. Tight to open folds are attributed to these deformation phases, as well as the development of discrete shear zones (Chemale et al., 1994; Rosière et al., 2001) during lower to medium greenschist metamorphic conditions. Superposition of structures of these two deformation episodes over older structures can be observed locally. A spaced and discrete crenulation cleavage developed during the second and third generation of fold axial planes (S_2 and S_3) with limited growth of platy hematite. The intersection lineation observed in itabirite and hematitites, resulting from the cross-cutting relationships between the foliations S_1 and S_2, is regionally subparallel to the stretching lineation observed in other rocks (quartzites, dolomitic marbles and itabirites) and indicate a tectonic transport to NE (Almeida et al., 2005).

We chose a decametric scale D_1 fold (Fig. 2) to investigate the variation of polycrystalline hematite microstructure and CPO. Fold geometry is defined by the interlayered compact and schistose hematite aggregates. In profile, the fold has a 1C class geometry (Ramsay, 1967). The interlimb angle is ~26°, the fold axis plunges 12° to NE, whereas the axial plane has a moderate dip to the southeast (Fig. 2). The fold lies in the hinge zone of a regional-scale isoclinal synform in the northeastern part of the Quadrilátero Ferrífero. Contractional and extensional structures in the internal and external hinge arcs were not observed, but the occurrence of "blue dust", which is hematite powder generated by the physical/mechanical breakdown of fine hematite plates into friable aggregates correlates to the external arcs of the fold. In both the fold limbs and hinge, a cross-cutting spaced cleavage S_2 oblique (~40°) to the folded foliation S_1 is present (Fig. 2) subparallel to the axial surface of the D_2 folds. The lineation from the intersection of the foliations is subparallel to the studied fold axis and it was interpreted as the *X*-tectonic direction, because regionally, the intersection lineation and the direction of maximum elongation of minerals are parallel. At the outcrop scale, L-type tectonites dominate in the fold hinge, whereas in the limbs, L-S types with some minor S-tectonites dominate.

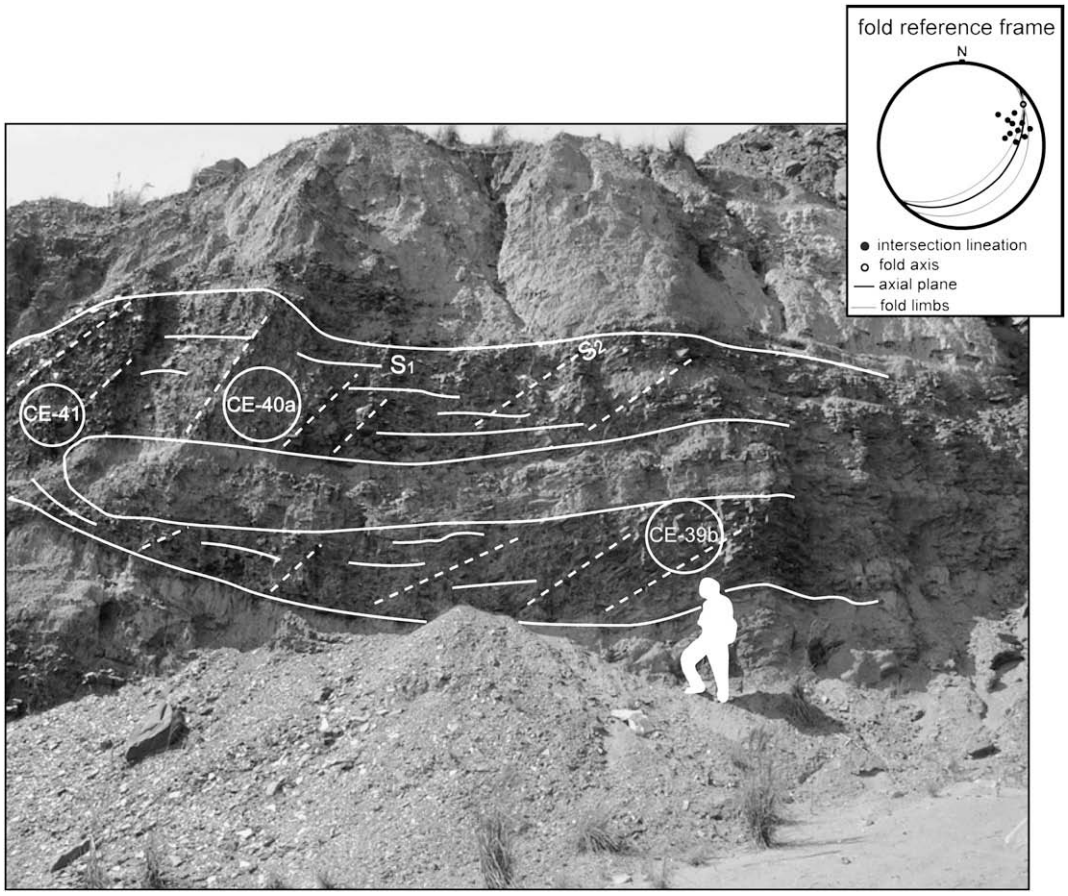

Fig. 2. Photograph of the studied fold and sample locations, showing the interlayering between schistose polycrystalline hematite (light gray) and hematitites (dark gray band, delineated by the white lines). View to the northeast, normal to the fold axis. The fold hinge line plunges 12° to NE, axial surface dips moderately to SE, interlimb angle is about 26°. Solid white lines mark the trace of axial surface foliation S_1, whereas dashed white lines mark the trace of the spaced cleavage S_2. The stereonet in the inset shows the orientation of the limbs, fold axis, axial surface, and the orientation of intersection lineations that regionally are parallel to the stretching lineation. N = number of measurements.

3. Methodology

3.1. Electron backscatter diffraction (EBSD)

The samples collected in the fold hinge and limb domains (Fig. 2) were oriented according to the tectonic reference frame *X*, *Y* and *Z*, where the *X*-axis is parallel to the intersection lineation, *Z* is normal to the foliation and *Y* is perpendicular to the *XZ* plane. The samples were cut perpendicular to the foliation and parallel to the lineation in blocks of dimensions $1.5 \times 1.5 \times 0.7$ cm. Then, they were mounted in epoxy and mechanically polished with diamond pastes of decreasing grain sizes. After this polishing, samples were ultra-polished with a diamond paste (0.25 μm) then with an alkaline solution of colloidal silica for 8–12 h, to remove residual surface damage and the topographic irregularities. As hematite crystals do not present charging problems in the SEM, no carbon coating was necessary.

The EBSD work was conducted using a JEOL SEM JSM5510, equipped with Nordlys HKL-Oxford EBSD detector operating at 20 keV and installed in the Laboratory of Microscopy and Microanalysis (MICROLAB), in the Department of Geology, Federal University of Ouro Preto. The EBSD data were acquired and indexed using the HKL Channel 5 software package. Preferred orientation measurements of hematite crystals were done via automatic beam scanning mode, with a step size of 10 μm in all samples, on a predefined area of $\sim 3500 \times 2750$ μm. The main setup parameters used in the present study were: tilt angle of 70°; working distance of 35 mm; spot size of 70; mean angular deviation (MAD) for data acquisition of 2°; MAD for pole figure calculation $\leq 1°$. The minimum and maximum number of detected bands was 4 and 5, respectively. Pattern-solving efficiencies for the indexed patterns were between 75% and 80%. The pole figures for [0001] axes and also for poles of $\{10\bar{1}0\}$ and $\{11\bar{2}0\}$ prisms, and $\{10\bar{1}4\}$ rhombs were calculated through the software PFch5 (Mainprice, 2007).

The orientation mapping was completed with through software Tango of the Channel 5 package. The zero solutions (misindexed or non-indexed points) were firstly reduced by the spike correction of individual zero-solution measurements relative to the surrounding points, and then by the extrapolation of successfully indexed patterns for the adjacent non-indexed/misindexed measurements. The latter procedure was carried out three times, giving the measurements of four well-indexed neighboring points, which is considered as a reasonable level to produce realistic microstructural maps for hematite aggregates. After the spike removing and extrapolation of successfully measurements to zero-solution points, the maps reach 90% of coverage in average, which means that 10% of the maps are made of non-indexed/misindexed points whose MAD number were higher than 2°. The strength of the pole figures was defined by the progressive increase of pfJ values index (Michibayashi and Mainprice, 2004). The pfJ value equals 1 when the fabric has a random distribution, and has maximum values dependent on the crystalline symmetry. As the symmetry of (0001) planes is different from the symmetry of the planes $\{10\bar{1}0\}$, $\{11\bar{2}0\}$ and $\{10\bar{1}4\}$ of hematite (Fig. 4), the values of pfJ cannot be used in a direct comparison between strength of the four different pole figures of the same sample. However, they can be used for the

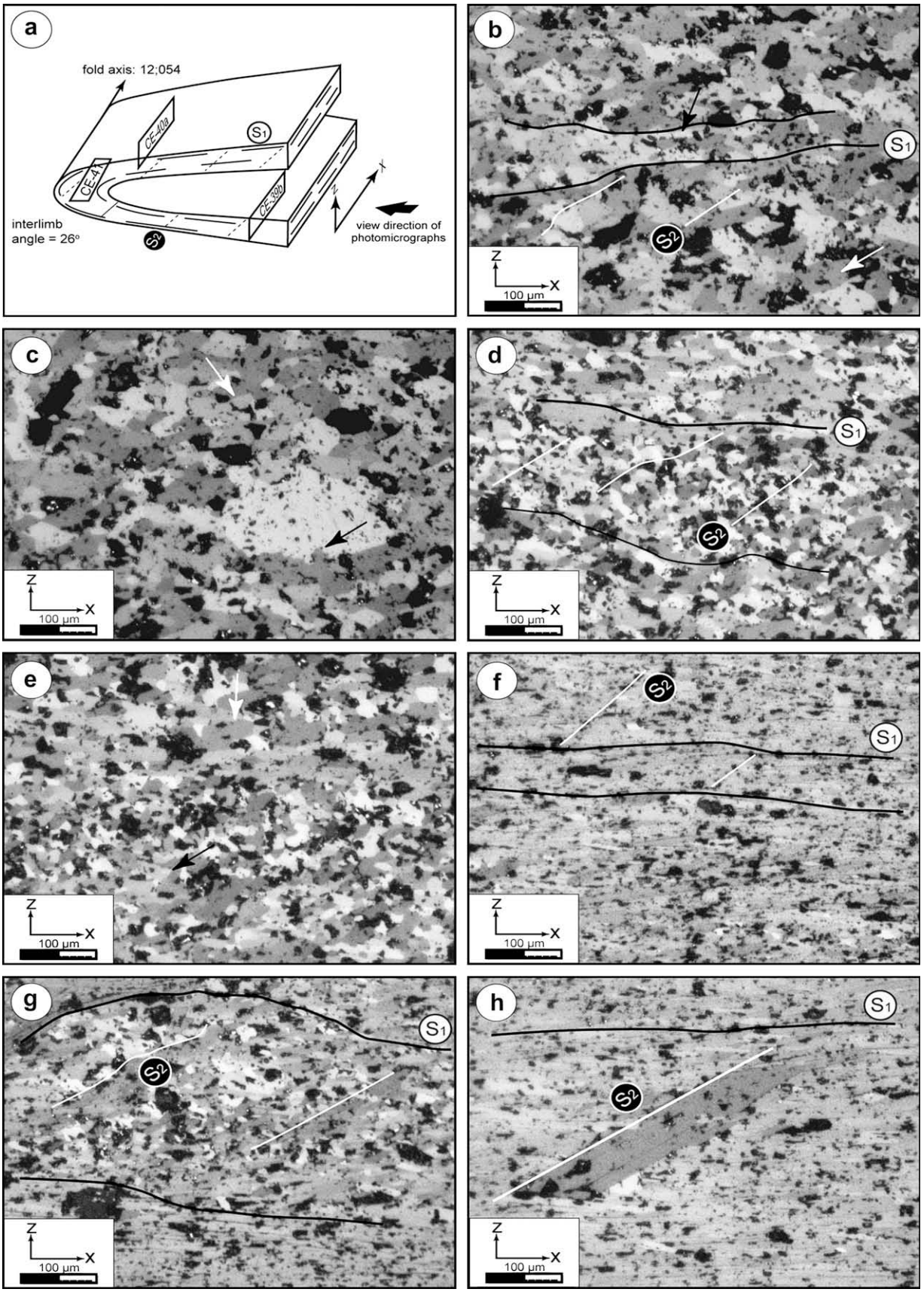

Fig. 3. Photomicrographs of the specimens collected in the limb (CE-39b, pictures b and c), transitional (CE-40a, pictures d and e) and hinge zone (CE-41, pictures f, g and h) of the studied fold (a). Solid black lines mark the axial surface foliation S_1, whereas solid white lines mark the spaced cleavage S_2. Cross polarized light. Arrows in (b) indicate granular (white arrow) and slightly flattened (black arrow) hematite crystals, whereas arrows in (c) indicate irregular (black arrow) and more regular (white arrow) contacts in coarse and fine-grained hematite grains, respectively. The black lines in (d) also mark the irregular boundaries of a granular hematite band (between the black lines) "sandwiched" between bands of platy-format hematite grains (above and below the black lines). White arrow in (e) indicates a regular grain boundary, whereas black arrow shows a lobate contact between hematite crystals. Black lines in (g) also mark the microlithon within the foliation of the specimen from the hinge. See text for details.

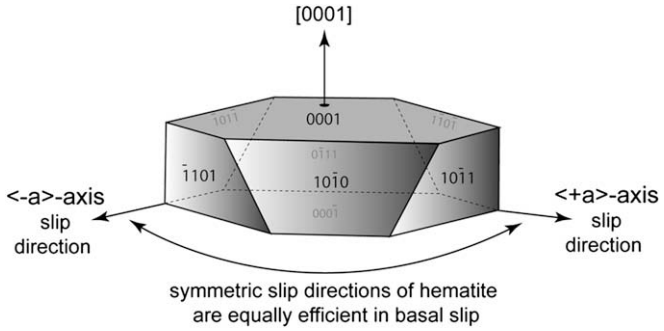

Fig. 4. Schematic representation of a plate-shaped hematite crystal, showing the basal and the main prismatic planes. The arrows represent the rotation of hematite *a*-axes around *c*-axis. Modified from http://webmineral.com/data/Hematite.shtml.

comparison of pole figures of same crystallographic planes or directions from different samples.

3.2. Grain size and shape properties

As the SEM/EBSD is a "single-grain" technique, it is possible to construct detailed grain-boundary maps for a given grain size if the setup accounts for the step size and the misorientation angles between grains. In the present study, grain boundaries were mapped to determine the crystal size distribution (CSD) of hematite grains and their variation around the studied fold. To map grain boundaries, a detailed beam scan was conducted in representative areas of ~600 × 500 μm, with step size of 2 μm, without any changes on the other parameters described above. The maps were constructed first by spike correction and removal of non-indexed/misindexed points as defined earlier. All interpreted grains smaller than four times the step size were discarded, appearing in the maps as zero-solutions. After that, zero-solutions were removed to produce the final grain-boundary maps, reaching coverage levels of 95%. The misorientation angle used in the grain-boundary mapping was 10°, which means that subgrain boundaries were disregarded. After all filtering processes, the grains were detected again and the resultant table with specifications of grains properties was statistically treated using the software "CSD corrections 1.37" (Higgins, 2000, 2002) assuming grains as 2D semi-ellipses. The mean grain-aspect ratio was determined using the program "Ellipstat" (Yamaji, 2005) from the data of long and short axis means obtained in the CSD correction program. The CSD corrections for the intersection probability and cut effect was determined, allowing for mean shape ratio of the grains (0.4) and the type and strength of the mesoscopic fabric of each sample.

4. Microstructures

The specimens (Fig. 3a) present a remarkable microstructural contrast between limbs and hinge zone.

4.1. Limb domain

In the limb (sample CE-39b), the foliation comprises the alignment of both granular and slightly flattened hematite grains (Fig. 3b). Grain boundaries are dominantly interfaces between hematite crystals and a few interphases between relicts of magnetite and hematite grains. Interfaces are usually straight and sharp in more rounded crystals, resulting in a polygonal network of grain

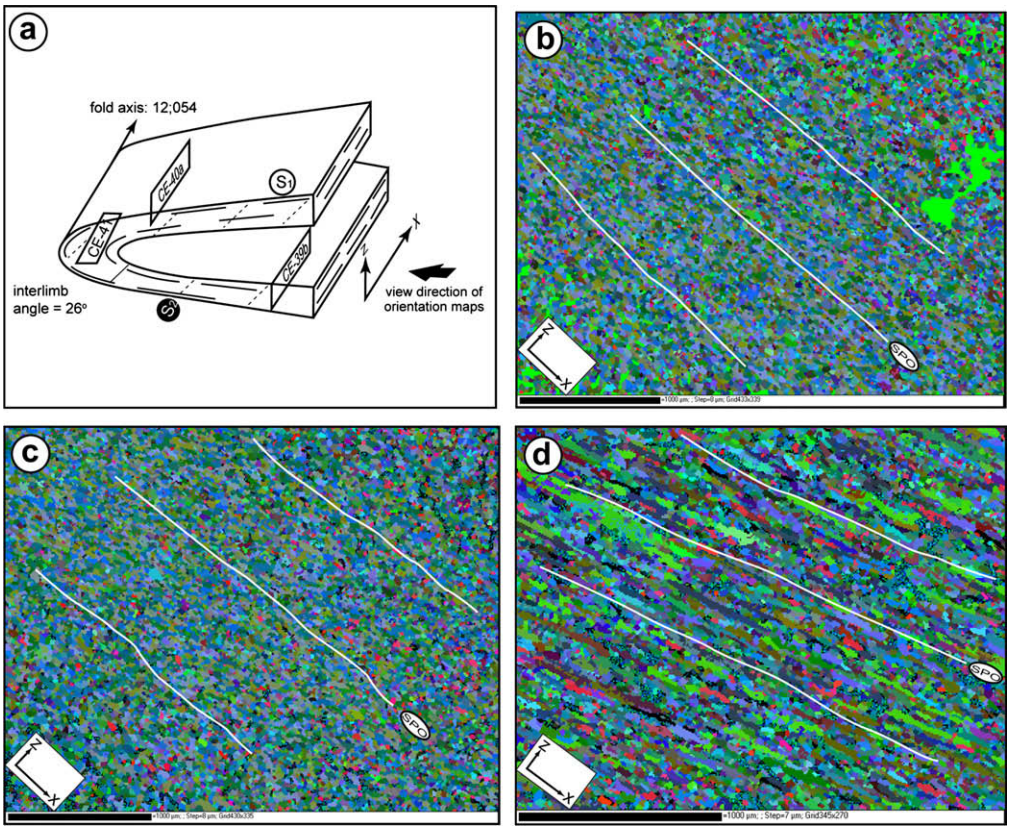

Fig. 5. EBSD maps, showing all Euler angles. In these maps, variations of colors represent variations on the crystallographic orientation of the minerals. Map (b) is for the sample CE-39b from the limb, (c) for the CE-40a in transitional domain and (d) for sample CE-41 from the hinge. Solid white lines indicate the presence of a shape-preferred orientation (SPO), which was visually determined. Maps were generated through the software Tango in the Channel 5 software package. Details in the text.

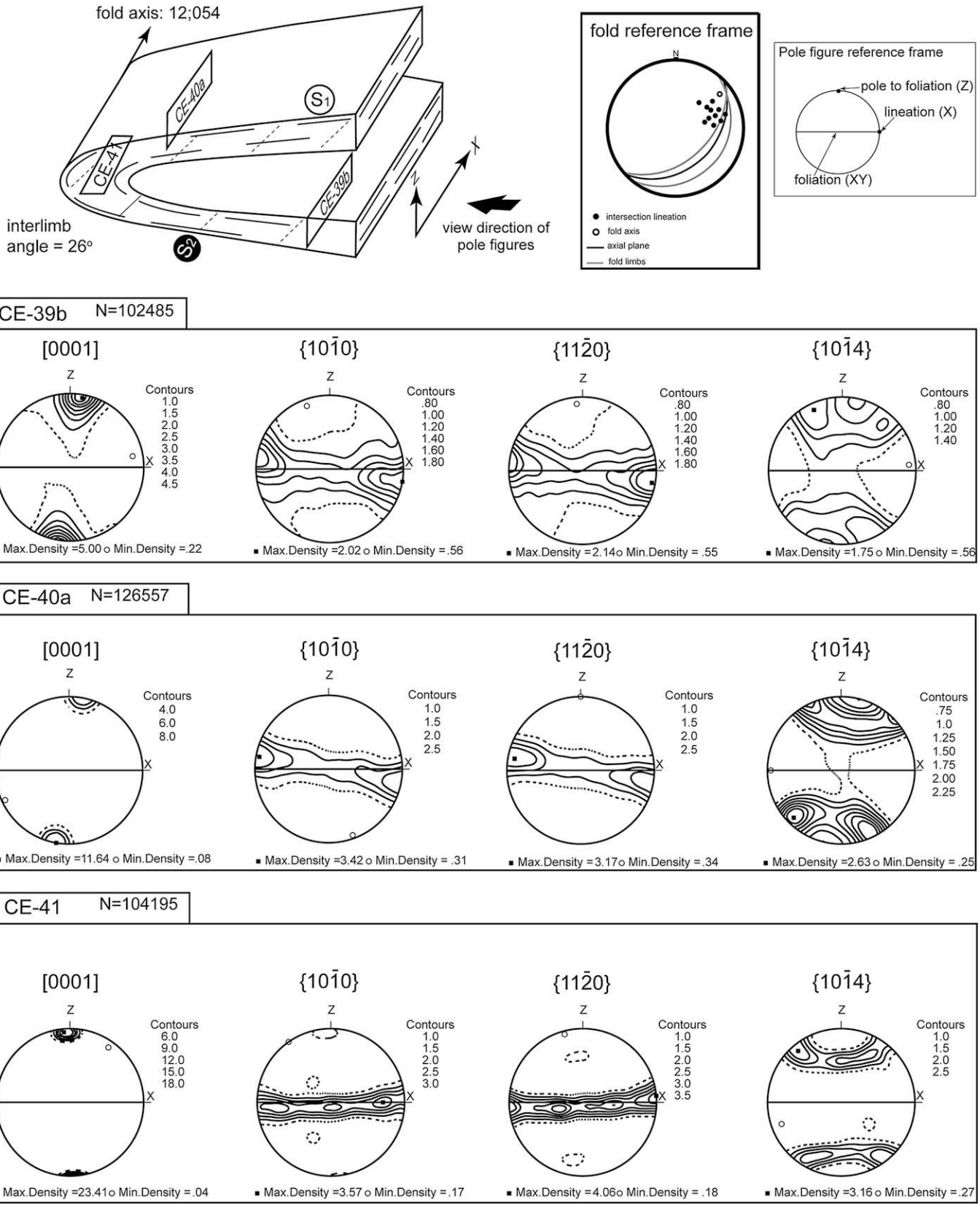

Fig. 6. Calculated pole figures for [0001] axes, poles of {10$\bar{1}$0} and {11$\bar{2}$0} prisms and {10$\bar{1}$4}. Pole figures calculated from Euler angles using the program PFch5 (Mainprice, 2007), lower hemisphere, multiples of uniform distribution, non-polar projection.

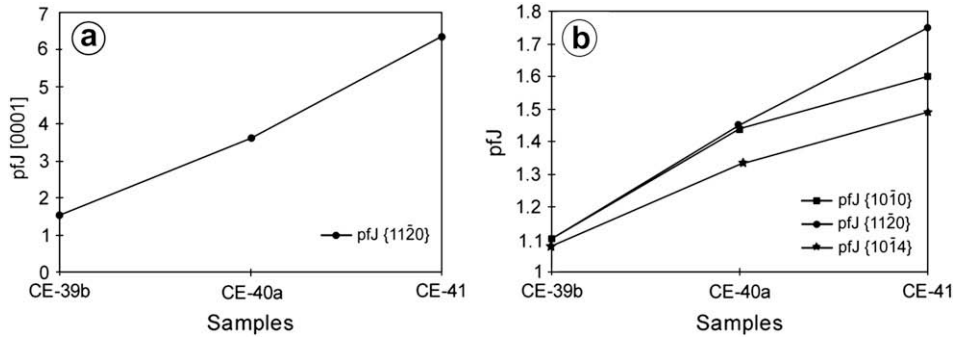

Fig. 7. Variation of pole figure sharpness (pfJ) showing the increase of CPO strength towards the fold hinge, from CE-39b to CE-41, for [0001] in (a) and for the poles to {10$\bar{1}$0}, {11$\bar{2}$0} and {10$\bar{1}$4} in (b). pfJ values were calculated trough the program PFch5 (Mainprice, 2007).

boundaries. However, relatively large hematite (>60 μm) grains show more irregular contacts (Fig. 3c).

4.2. Transitional domain

The foliation in the transition zone of the fold (sample CE-40a) comprises alternating platy and granular hematite grains, which occur in regular millimetric layers with strong alignment of hematite plates parallel to the foliation (Fig. 3d). Grain boundaries of hematite crystals are usually sharp and straight (Fig. 3e). In more granular hematite, irregular and polygonal segment boundaries are relatively common. Locally, porphyroclasts of polycrystalline granular hematite with symmetric tails of tabular hematite are observed.

4.3. Hinge zone

In the hinge zone (sample CE-41), a strong shape preferred orientation (SPO) of hematite plates parallel to the fold axis is observed (Fig. 3f). Granular hematite crystals are scarce and limited to lens shaped domains between the foliation planes, interpreted here as microlithons (Fig. 3g). In these domains, shape orientations of granular and platy hematite are weaker than those in the foliation domains. In general, interface hematite–hematite boundaries are dominantly sharp and straight, and irregular boundaries are restricted to granular hematite within microlithons. Sparse magnetite crystals are also restricted to the microlithons. In all samples, the oblique foliation S_2 consists of a spaced cleavage marked by hematite plates regularly spaced throughout the fold (Fig. 3h). The cleavage planes are more clearly visible in the hinge zone, but in all samples they make an angle of ~40° with the folded foliation S_1.

5. CPO analyses

The sampled CPOs (Fig. 5) are similar in geometry around the folded layer. The poles of the basal planes of hematite are concentrated close to the foliation normal, whereas the poles of prismatic planes are distributed in a girdle along the foliation, with a tendency for concentration parallel to *X* (Fig. 6). The poles of the rhomb planes {10$\bar{1}$4} distribute along a conical girdle around the foliation normal (Fig. 6).

The CPO patterns intensify toward the hinge zone (Fig. 6). In the limb domains, [0001] axes scatter between the foliation normal and the *Y*-direction (Fig. 6). Such a scattering is also observed in the pole figures of prismatic planes {10$\bar{1}$0} and {11$\bar{2}$0}, where the girdle parallel to the foliation is relatively wide, scattering from the foliation plane toward the foliation normal. The conical girdle distribution of {10$\bar{1}$4} poles is also wide and not well-developed in the limb. Towards the hinge, the concentration of [0001] becomes stronger and the girdles for both prismatic and rhomb poles become narrower and sharper (Fig. 6). The concentrations of the crystallographic axes in the sample from the hinge zone (CE-41) are so strong that the CPO patterns can be almost described as a "single crystal" preferred orientation. Despite the scattering along the foliation, the maximum concentration of poles of {10$\bar{1}$0} and {11$\bar{2}$0} planes tend to be systematically parallel to the *X*-direction (Fig. 6) in all specimens. The small obliquity of the pole figures is likely an artifact caused by sectioning because we did not observed any asymmetric microstructure, neither in the limbs nor in the hinge of the studied fold. The value of pfJ, quantifying the strength of the crystallographic fabric increases substantially from the limb towards the hinge zone, principally for the [0001] axes, which are strongly concentrated in the hinge of the fold (Fig. 7), along with increasing concentrations of {10$\bar{1}$0}, {11$\bar{2}$0} and {10$\bar{1}$4} poles, although 10 times lower in magnitudes than for [0001].

6. Grain size and shape properties

The average grain size is ~16 μm in the limb (Fig. 8a and b) increasing to 20 μm toward the hinge (Fig. 8d and e), and reaching 30 μm in average in the hinge zone itself (Fig. 8g and h). In all samples, the grain size variation is rather small, although larger in the hinge. The increase in grain size and size variation is matched by an increase in grain aspect ratio from 2.25 in the limbs to 4 toward the hinge (Fig. 8c, f and i). Although the average grain aspect ratio in the hinge is 4, individual grains reached aspect values of 9 (Fig. 8i). All these characteristics confirm that the fold hematite-related fabrics vary along the fold, and become progressively stronger towards the hinge zone. Regardless of the differences in shape fabric between limbs and hinge of the studied fold, long axes of the elongate hematite grains also preferentially aligns parallel to the fold axis.

7. Discussion

The CPO data suggested that hematite grains were deformed by intracrystalline deformation. From the pole figures it can be inferred that the main active slip system was basal in <a> direction because the strong concentration of [0001]-axes parallel to *Z* and the distribution of poles of prismatic forms parallel to the foliation. This is in agreement with the results of Rosière et al. (1998, 2001) and Siemes et al. (2000) for hematite deformation at these conditions. Such a distribution pattern also indicate that the six symmetric <a>-directions of hematite were equally efficient as slip direction and allow the development of a crystallographic fabric parallel to the foliation of reference frame (Fig. 6). The activation of different slip <a>-directions is very clear on the pole figures of

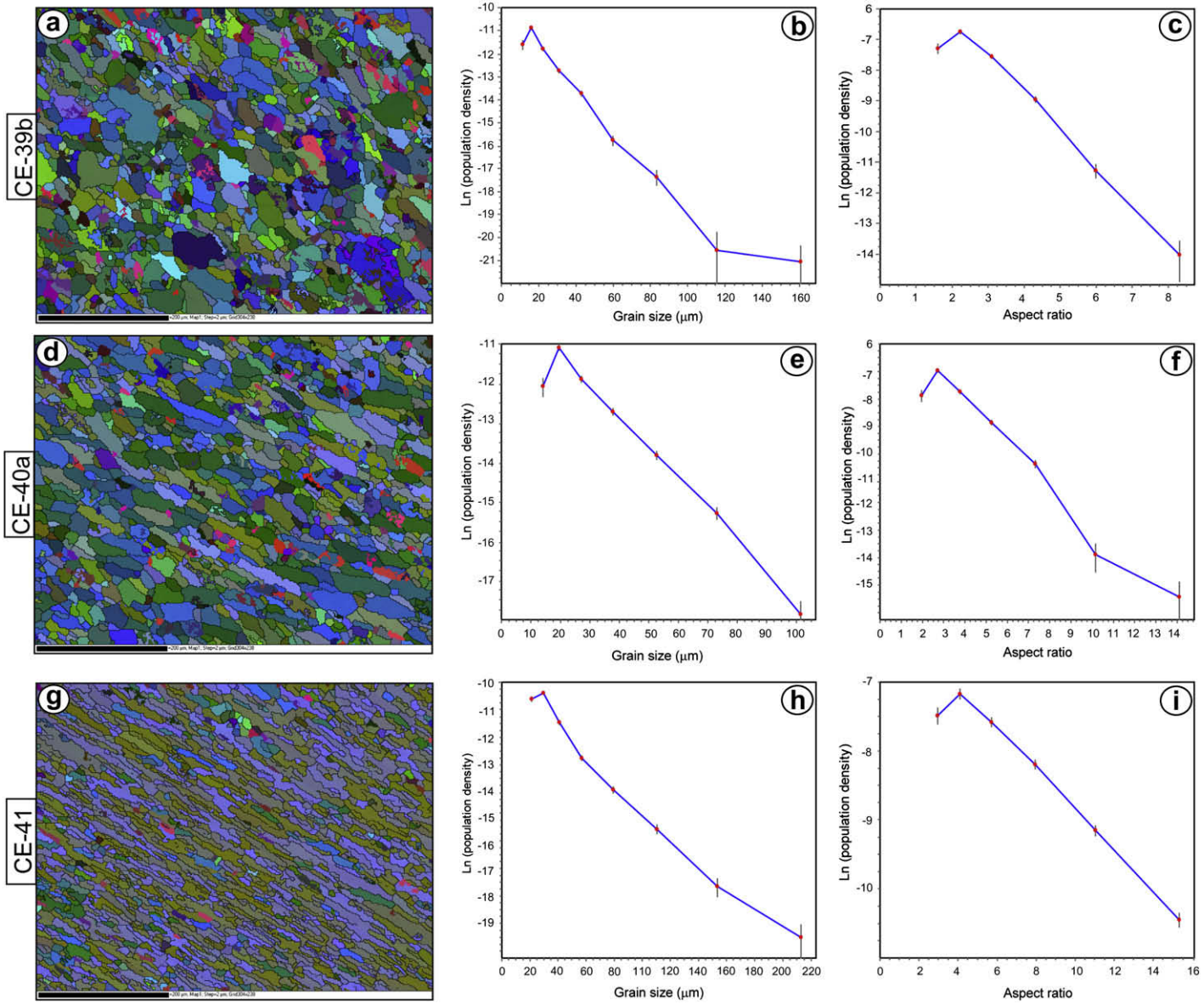

Fig. 8. Detailed Euler angles and grain boundaries maps (a, d, g), crystal size distribution (b, e, h) and aspect ratio plots (c, f, i) for the samples CE-39b, CE-40a and CE-41. In the maps, different colors represent different orientations. Crystal size distribution for grains ≥8 μm. Detected grain boundaries for misorientation angles ≥10°. Ln (population density) in the *y*-axes is the volumetric number density divided by the width of the interval, following Higgins (2000).

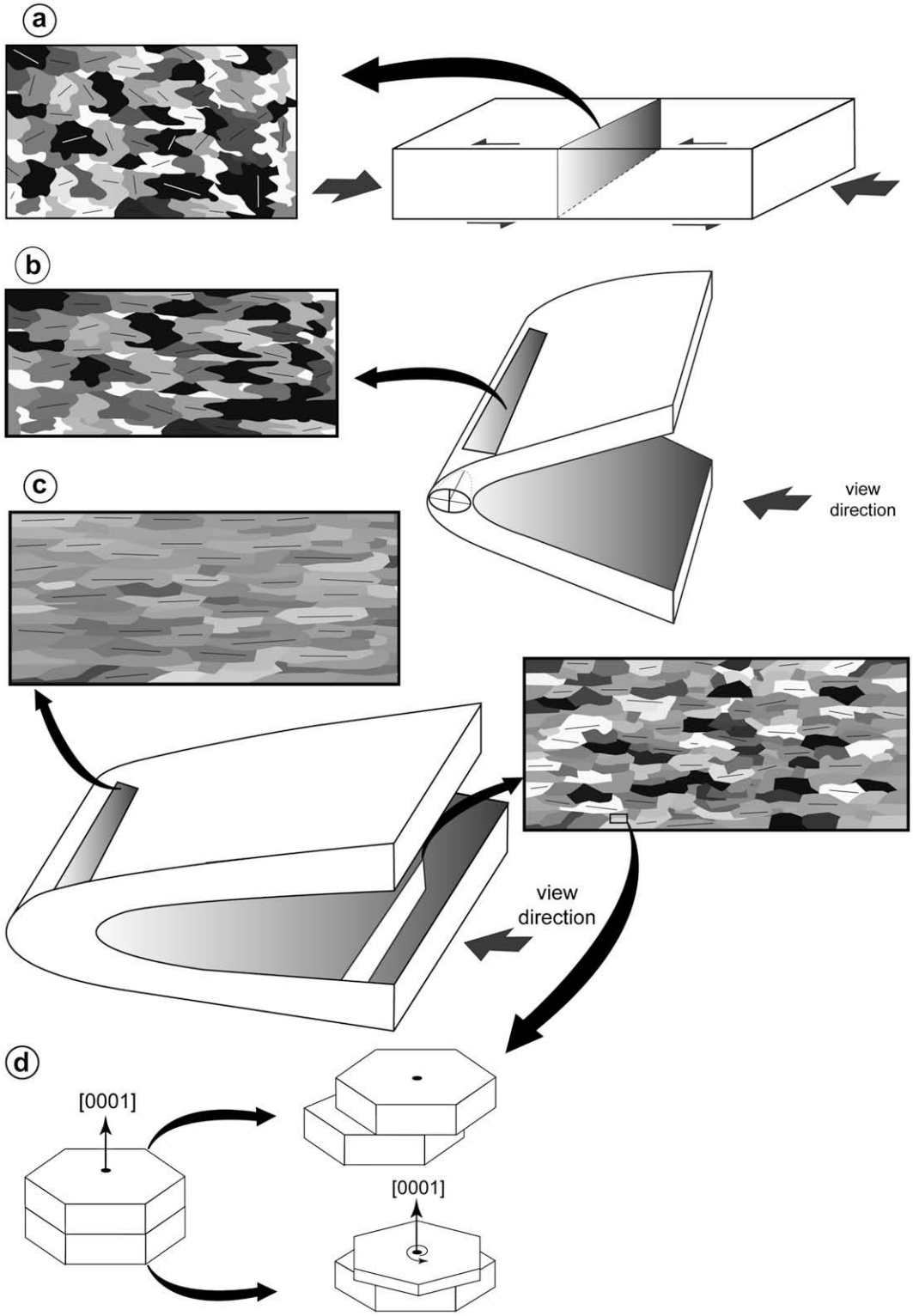

Fig. 9. Sketch showing a time sequence of progressive flattening and elongation of hematite grains and the increase in aspect ratio in the fold hinge, as well as the rotation of hematite basal planes (solid lines within the grains) during the progressive tightening of the structure (a, b and c). Different shades of gray illustrate the differences in orientations. The sketch in (d) illustrates possible grain boundary sliding or rotation along basal boundaries of two neighboring hematite grains.

poles to prismatic planes from the sample CE-41 (hinge zone), where three similar maximum contour lines are observed (Fig. 6). A similar behavior is observed in the deformation of ice. During a progressive simple shear deformation, the *c*-axes of ice crystals develop two single maxima linked by a girdle centered in the *Y*-direction of the pole figure. These two single maxima lie at an angle about 30° in relation to the pole of foliation in the tectonic reference frame. As shear strain increases, the metastable orientation maxima disappears, becoming a single *c*-axes maxima that progressively becomes orientated parallel to shortening direction of the pole figure (*Z*-axis). In such a position, the basal planes of ice are orientated parallel to the bulk shear plane of the sample (Bouchez

and Duval, 1982; Urai et al., 1986; Wilson, 1986). In this case, the easy activation of basal slip results from six symmetric slip directions due to the hexagonal symmetry of ice crystals, allowing the development of a strong girdle of poles of prismatic planes parallel to the foliation in the reference frame. The observed scattering in the pole figures can represent: (i) the presence of granular hematite crystals with basal planes not parallel/subparallel to the foliation; (ii) a crenulated foliation, or (iii) the consequence of intersection between the foliation (S_1) and cleavage planes (S_2) (Rosière et al., 2001). In the present study, the pattern of scattering results from both strain distribution around the fold and from the presence of cross-cutting S_1 and S_2 planes, observed both in the field as well as in thin sections (Figs. 2 and 3).

During the tightening of the fold, flow probably occurs as layer-parallel shear toward the hinge, and the deformation are used to infer the activation of flexural flow, leading to the transition in fabric characteristics from limb to hinge. Such a process will cause the SPO to be stronger in the hinge domains. The increase of grain shape anisotropy towards the fold hinge is followed by progressive strengthening of hematite [0001] axes maxima around the foliation normal. In addition, the sharpness of girdles of poles of prismatic planes arranged in an elongated maximum parallel to the foliation plane and the progressive increasing increase of pfJ values in the same direction are used to infer that strain was preferentially accommodated in the hinge zone (e.g. Ramsay, 1967; Hudleston and Lan, 1993). With the progressive shortening of the initial hematite grains in one direction and respective elongation in one or two directions, and with the bulk rotation, it is likely that some grain boundary sliding (GBS) may have occurred during deformation (Fig. 9). The operation of GBS is facilitated by the strong shape anisotropy of hematite grains of basal habits and by the presence of fluids during deformation, which was common over the QF areas and evidenced in the studied fold by the extensive breakdown of magnetite to hematite (Lagoeiro, 1998). The operation of GBS allows the sliding and the rotation of hematite crystals mainly along the basal boundaries (Fig. 9). As these processes occurred preferentially along the basal- instead of prismatic- or rhomb-planes, the aggregates retained the existing CPO produced by basal intracrystalline slip. In fact, basal intracrystalline slip in <a>-direction of hematites, or the rotation of hematite plates along basal grain boundaries, with a rotation axis parallel to [0001] (Fig. 9) would lead to a similar preferred orientation pattern. Thus, in this case, the CPO would be insensitive to the deformation mechanism. Therefore, detailed experimental deformation work with transmission electronic microscopy analyses is required to improve understanding about hematite deformation mechanisms.

8. Summary and conclusions

Intracrystalline deformation of hematite grains occurred by basal slip in the <a>-direction, leading to the development of a relatively strong CPO. In both the hinge and limb the main fabric consists in a maximum of [0001] axes around the normal to foliation (*Z*), with the poles of prismatic planes concentrated along the foliation plane. However, the maximum of [0001]-axes observed in the hinge zone is close to a point maximum, whereas in the limbs the concentrations are broader around *Z*-axis. The same trend is also observed with respect to the poles to prismatic planes: in the limbs they tend to distribute in a wide girdle along the foliation plane, whereas in the hinge zone they distribute in a narrow girdle, as also attested by pfJ values. The increase in the strength of the CPO is also reflected in the grain shape fabric, which in the limbs is slightly less anisotropic than in the hinge, although just a slight increase in grain size is observed towards the hinge. Combining the crystallographic and shape fabrics together with the field observations, we conclude that accommodation of deformation varied along the fold domains. In the hinge, the narrower dispersion of crystallographic orientation of prismatic poles, the larger aspect ratio and the alignment of long axis of elongate grains parallel to the fold axis indicate that flow intensity from the limbs during folding yielded more intense structural fabric in the hinge zone. On the other hand, in the limbs deformation was less intense, producing less intense preferred orientations and weakly flattened grains. Additional deformation mechanisms such as bulk rotation of hematite grains, as well as grain boundary sliding, might have accommodated deformation in the studied fold. The hematite grains may also have rotated around their [0001]-axes, in a similar manner to the rotation of mica plates along their cleavage planes. Such a rotation was accompanied by grain flattening, assisting the creation of a stable geometry to reflect overall flattening within the fold hinge. The grain-boundary sliding was facilitated by the shape anisotropy of hematite grains as well as by the presence of an aqueous fluid phase without any microstructure indicative of microfracturing.

Acknowledgments

The authors gratefully acknowledge Alan P. Boyle and Neil Mancktelow for the very helpful comments and suggestions on the first version of this manuscript. The reviews of Professor Jean-Luc Bouchez and an anonymous referee, as well as the editorial handling of Professor William M. Dunne helped to improve the final version of this paper. David Mainprice is thanked for providing the software PFch5. We also express our gratitude to Leonardo E.G. da Silva and Cristiane Castro for the assistance in the preparation of the samples. L.F.G.M. is grateful to Conselho Nacional de Pesquisa e Desenvolvimento (CNPq—51648/2006-9) and Fundação de Amparo à Pesquisa no Estado de Minas Gerais (FAPEMIG—CRA00185/0).

References

Alkmim, F., Marshak, S., 1998. Transamazonian orogeny in the southern São Francisco craton region. Minas Gerais, Brazil: evidence for Paleoproterozoic collision and collapse in the Quadrilátero Ferrífero. Precambrian Research 90, 29–58.

Almeida, L.E., Castro, P.T.A., Endo, I., Fonseca, M.A., 2005. O Grupo Sabará no Sinclinal Dom Bosco, Quadrilátero Ferrífero: Uma revisão estratigráfica. Revista Brasileira de Geociências 35 (2), 177–186.

Babinski, M., Chemale, F., Van Schmus, W.R., 1995. The Pb/Pb age of Minas Supergroup carbonate rocks, Quadrilátero Ferrífero, Brazil. Precambrian Research 72, 235–245.

Bouchez, J.-L., Duval, P., 1982. The fabric of polycrystalline ice deformed in simple shear: experiments in torsion, natural deformation and geometrical interpretation. Textures and Microstructures 5, 171–190.

Chemale Jr., F., Rosière, C.A., Endo, I., 1994. The tectonic evolution of the Quadrilátero Ferrífero, Minas Gerais, Brazil. Precambrian Research 65, 25–54.

Cogné, J.P., Gapais, D., 1986. Passive rotation of hematite during deformation: a comparison of simulated and natural redbeds fabrics. Tectonophysics 121, 365–372.

Hennig-Michaeli, C., 1977. Microscopic structure studies of experimentally and naturally deformed hematite ores. Tectonophysics 39, 255–271.

Higgins, M.D., 2000. Measurement of crystal size distribution. American Mineralogist 87, 1105–1116.

Higgins, M.D., 2002. Closure in crystal size distributions (CSD), verification of CSD calculations and the significance of CSD fans. American Mineralogist 87, 171–175.

Hoefs, J., Müller, G., Schuster, A.K., 1982. Polymetamorphic relations in iron ores from the Iron Quadrangle. Brazil: The correlation of oxygen isotope variations with deformation history. Contributions to Mineralogy and Petrology 79, 241–251.

Hudleston, P.J., Lan, L., 1993. Information from fold shapes. Journal of Structural Geology 15 (3-5), 253–264.

Ji, S., Salisbury, M., Hanmer, S., 1993. Petrofabric, P-wave anisotropy and reflectivity of high-grade tectonites. Tectonophysics 222, 195–226.

Lagoeiro, L., 1998. Transformation of magnetite to hematite and its influence on the dissolution of iron oxide minerals. Journal of Metamorphic Geology 16, 415–423.

Lagoeiro, L., Hippertt, J., Lana, C., 2003. Deformation partitioning during folding and transposition of quartz layers. Tectonophysics 361, 171–186.

Law, R.D., Schmid, S.M., Wheeler, J., 1990. Simple shear deformation and crystallographic fabrics: a possible natural example from the Torridon area of NW Scotland. Journal of Structural Geology 12 (1), 29–45.

Lloyd, G.E., Law, R.D., Mainprice, D., Wheeler, J., 1992. Microstructural and crystal fabric evolution during shear zone formation. Journal of Structural Geology 14, 1079–1100.

Mainprice, D., 2007. ftp://www.gm.univ-montp2.fr/mainprice//CareWare_Unicef_Programs/.

Michibayashi, K., Mainprice, D., 2004. The role of pre-existing mechanical anisotropy on shear zone development within oceanic mantle lithosphere: an example from the Oman ophiolite. Journal of Petrology 45 (2), 405–414.

Morales, L.F.G., Hinrichs, R., Fernandes, L.A.D., 2007. A Técnica de difração de elétrons rétro-espalhados (EBSD) em um microscópio eletrônico de varredura (MEV) e sua aplicação no estudo de rochas deformadas. Revista Pesquisas em Geociências 34 (1), 19–34.

Nicolas, A., Poirier, J.-P., 1976. Crystalline Plasticity and Solid State Flow in Metamorphic Rocks. John Wiley and Sons, New York.

Pires, F.R.M., 1995. Textural and mineralogical variations during metamorphism of the Proterozoic Itabira Formation in the Quadrilátero Ferrífero, Minas Gerais, Brazil. Anais da Academia Brasileira de Ciências 67, 77–105.

Prior, D.J., Boyle, A.P., Brenker, F., Cheadle, M.C., Day, A., Lopez, G., Potts, G.J., Reddy, S., Spiess, R., Timms, N., Trimby, P., Wheeler, J., Zetterstrom, L., 1999. The application of electron backscatter diffraction and orientation contrast imaging in the SEM to textural problems in rocks. American Mineralogist 84, 1741–1759.

Ramsay, J.G., 1967. Folding and Fracturing of Rocks. McGraw Hill, New York.

Randle, V., 1992. Microtexture Determination and its Applications. The Institute of Materials, London.

Rosière, C.A., Quade, H., Siemes, H., Chemale Jr., F., 1998. Fabric, texture and anisotropy of magnetic susceptibility in high-grade iron ores from the Quadrilátero Ferrífero, Minas Gerais, Brazil. Materials Science Forum, 273–275. 693-700.

Rosière, C.A., Siemes, H., Quade, H., Brokmeier, H.-.G., Jansen, E.M., 2001. Microstructures, textures and deformation mechanisms in hematite. Journal of Structural Geology 23, 1429–1440.

Schmid, S.M., Casey, M., 1986. Complete fabric analysis of some commonly observed quartz c-axis patterns. In: Hobbs, B.E., Heard, C. (Eds.), Mineral and Rock Deformation: Laboratory Studies—The Paterson Volume. American Geophysical Union, pp. 263–286. Geophysical Monograph 36.

Siemes, H., Hennig-Michaeli, Ch., 1985. Ore minerals. In: Wenk, H.-R. (Ed.), Preferred Orientation in Deformed Metals and Rocks: An Introduction to Modern Texture Analysis. Academic Press, London, pp. 335–360.

Siemes, H., Schaeben, H., Rosière, C.A., Quade, H., 2000. Crystallographic and magnetic preferred orientation of hematite in banded iron ores. Journal of Structural Geology 22 (11/12), 1747–1761.

Urai, J.L., Means, W.D., Lister, G.S., 1986. Dynamic recrystallization of minerals. In: Hobbs, B.E., Heard, C. (Eds.), Mineral and Rock Deformation: Laboratory Studies—The Paterson Volume. American Geophysical Union, pp. 161–199. Geophysical Monograph 36.

Wilson, C.J.L., 1986. Deformation induced recrystallization of ice: the application of in situ experiments. In: Hobbs, B.E., Heard, C. (Eds.), Mineral and Rock Deformation: Laboratory Studies—The Paterson Volume. American Geophysical Union, pp. 213–232. Geophysical Monograph 36.

Yamaji, A., 2005. Finite tectonic strain and its error, as estimated from elliptical objects with a class of initial preferred orientations. Journal of Structural Geology 27, 2030–2042.